Mechanism and Machine Theory xxx (2015) xxx–xxx

Contents lists available at ScienceDirect

Mechanism and Machine Theory

journal homepage: www.elsevier.com/locate/mechmt

Unified kinematics and optimal design of a 3rR*PS* metamorphic parallel mechanism with a reconfigurable revolute joint

Dongming Gan [a,b,*], Jorge Dias [a,c], Lakmal Seneviratne [a,b]

[a] Robotics Institute, Khalifa University of Science, Technology & Research, 127788 Abu Dhabi, United Arab Emirates
[b] School of Natural and Mathematical Sciences, King's College London, University of London, London WC2R2LS, UK
[c] Institute of Systems and Robotics, University of Coimbra, Faculty of Science and Technology, Coimbra, Portugal

ARTICLE INFO

Available online xxxx

Keywords:
Reconfiguration
Unified kinematics
Singularity-free workspace
Optimization
Parallel mechanism

ABSTRACT

This paper introduces a new metamorphic parallel mechanism based on a reconfigurable revolute (rR) joint and the mechanism consists of three rR*PS* (rR joint-prismatic joint-spherical joint) limbs. Reconfiguration principle of the rR joint and the rR*PS* limb is explained, based on which the 3rR*PS* metamorphic parallel mechanism can be reconfigurable between two working motion types, pure rotation (3R) motion and one translation and two rotation (1T2R) motion. Using the limb geometric constraint model, analytical forward kinematics is solved in a unified way for both motion types. Reciprocal screw based Jacobian is obtained for singularity analysis which is then used for singularity-free workspace analysis. Based on those, maximum singularity-free workspace and kinematics performance based criteria are applied in optimizing basic mechanism parameters considering input and passive joint limitations. A unified objective function with variable design priorities represented by function weights of the two topologies is proposed and examples are illustrated. The introduced new parallel mechanism covers the two very useful motion types, 3R and 1T2R, while the model in the paper provides basis of modeling and optimal design for further applications.

1. Introduction

Parallel mechanisms have been successfully applied as tire test machine [1], industry assembly tools [2], manufacturing center [3], force transducer [4], rehabilitation platform [5] and robotics surgery instrument [6] due to their high load-carrying capacity, good positioning accuracy and low inertia [7] stemmed from their multi-loop geometric structures [8]. Due to fast task change with variable mobility requirements, like rapid customization and diverse environment changing [9], rehabilitation and surgery of different human joints, parallel mechanisms which are reconfigurable have attracted much interest from mechanism researchers. Based on this, metamorphic parallel mechanisms (MPMs) [10], which are a class of mechanisms that possess adaptability and reconfigurability to change permanent finite mobility based on topological structure change, were introduced. Metamorphic parallel mechanisms have all the advantages of traditional parallel mechanisms [11] but with ability of reconfiguring for mobility change.

In this paper, a new metamorphic parallel mechanism with a reconfigurable revolute joint is proposed. The new mechanism has the ability of mobility change between 3R motion and 1T2R motion which are the two very useful motions in parallel mechanism applications and the two widely studied motion types in parallel mechanism research. Novel applications of parallel mechanisms with 3R motion include camera orienting devices [12], robotic joints [13,14], robotic surgery platform [15], and human joint rehabilitation [16]. Parallel mechanisms with 1T2R motion have been applied as flight simulator [17], micro-medical device [18], coordinating–

* Corresponding author at: Robotics Institute, Khalifa University of Science, Technology & Research, 127788 Abu Dhabi, United Arab Emirates. Tel.: +971 2 5018558; fax: +971 2 4472442.
E-mail address: dongming.gan@kustar.ac.ae (D. Gan).

http://dx.doi.org/10.1016/j.mechmachtheory.2015.08.005
0094-114X/

measuring machine [19] and machining tools [2,20]. However, those two types of parallel mechanisms were treated independently with case-by-case applications. The new metamorphic parallel mechanism proposed in this paper can provide both motion types with the same mechanical structure. This keeps kinematics and dynamics simplicity of lower-DOF parallel mechanisms but provides capability to multi-tasks, like machining different types of components, and rehabilitation of different human joints. The study of this paper will illustrate the reconfiguration concept, unified kinematics analysis and optimal design of the new parallel mechanism, which can be used for the mechanism design and applications. More than that, the proposed reconfiguration method can also be extended to generate more reconfigurable parallel mechanisms.

Current mechanism research shows some basic ways to design reconfigurable mechanisms. One is to change the number of links by link coincidence and self-locking as in [21–24]. It was used in proposing metamorphic mechanisms in the study of decorative carton folds and reconfigurable packaging [21]. Later, a metamorphic multifingered hand with an articulated palm by link coincidence of a spherical five bar linkage was presented [22]. A general approach for self-locking analysis was done in [23] while various joint types were explained and used in kinematic representations of metamorphic pop-up paper mechanisms in [24].

Another way of reconfiguration is through singularities. One of the cases is to have bifurcated configurations through constraint singularities [25]. Kinematotropic mechanisms were the earliest mechanisms that the permanent mobility could be changed after it passed through the singular positions [26]. Following the study of single-loop and multi-loop kinematotropic mechanisms, parallel mechanisms with bifurcated motion were also constructed [27]. Using the same principle, a parallel mechanism with changed motion for machine tool applications was proposed [28] while a family of parallel mechanisms that have multiple operation modes were presented [29,30]. Using linear transformations, new 1R2T parallel mechanisms with a bifurcated rotation motion on two orthogonal directions [31] were synthesized. In addition to constraint singularities, through both Type 1 [32] and Type 2 [33] singularities, parallel mechanisms can be also reconfigured between different motion types.

Other methods of reconfiguring mechanisms include special trajectory planning [34], variable actuation modes [35,36] and variable geometric joints [10,37]. The last method is to apply geometric constraint to joints to change the joint property and has been recently developed a lot. Variable topologies of kinematic joints and their topological representation were presented in [37]. Based on a reconfigurable Hooke (rT) joint, various metamorphic parallel mechanisms [10,38] have been synthesized and a general construction method using screw theory was introduced [39]. Similarly a metamorphic parallel mechanism with the ability of performing phase change and orientation switch was proposed by introducing a metamorphic kinematic pair [40] and a class of metamorphic parallel mechanisms was designed using a variable-axis (vA) joint [41]. Recently, unified kinematics modeling and singularity analysis of metamorphic parallel mechanisms have been investigated in [42,43]. By designing a reconfigurable universal joint, a 3-CUP parallel mechanism was proposed to reconfigure into two motion types [44].

Using similar principle to the rT joint [10] and vA joint [41], this paper introduced a reconfigurable revolute (rR) joint of which the rotation axis can be altered freely on a plane. Based on this, three rR*PS* limbs are used to construct a metamorphic parallel mechanism which can change its platform mobility between 3-DOF spherical motion and 3-DOF 1T2R motion. This paper then shows a unified kinematics model for analytic solutions of the forward and inverse displacement analysis covering the two different motion types. Reciprocal screw based Jacobian matrix is also used to represent the singularity loci. Following this, a method of obtaining optimized structure parameters to have the maximum singularity-free workspace and good kinematics performance for both motion types is proposed.

In the following, the paper is arranged as: Section 2 introduces the reconfigurable revolute joint and the r*RPS* limb with its geometric constraint analysis in screw theory; following this, mobility change of the 3r*RPS* metamorphic parallel mechanism is demonstrated in Section 3 and unified kinematics analysis is solved in Section 4; over all Jacobian matrix in terms of reciprocal screws is derived to obtain singularity loci and singularity-free workspace is then illustrated in Section 5; based on these, parameter effect on maximum

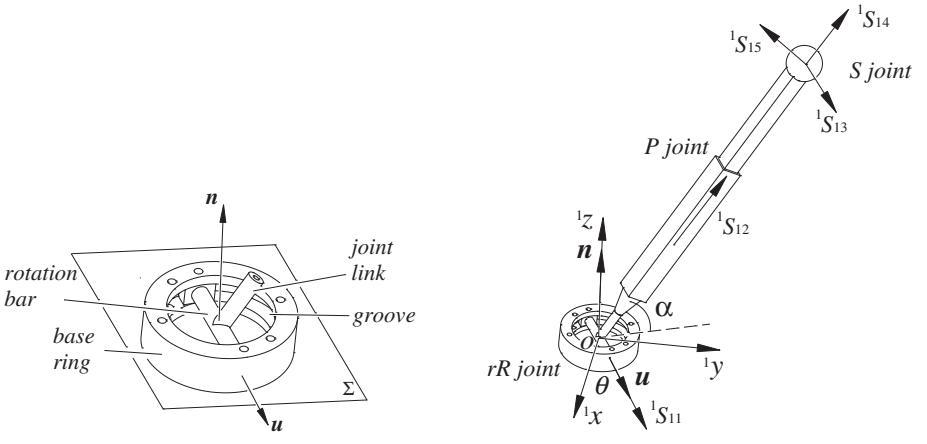

(a) rR joint (b) r*RPS* limb

Fig. 1. The rR joint and the r*RPS* limb.

Please cite this article as: D. Gan, et al., Unified kinematics and optimal design of a 3r*RPS* metamorphic parallel mechanism with a reconfigurable revolute joint, Mech. Mach. Theory (2015), http://dx.doi.org/10.1016/j.mechmachtheory.2015.08.005

singularity-free workspace is carried out in Section 6 and optimal design is then demonstrated in Section 7; reconfiguration strategy and the rT joint design are discussed in Section 8; conclusions make up Section 9.

2. The reconfigurable revolute (rR) joint and the rR*PS* limb

As in Fig. 1(a), the reconfigurable revolute joint, named rR joint, consists of a ring base, a rotation bar and a joint link. The joint link which is normally connected to a mechanism limb and perpendicular to the rotation bar rotates about the rotation bar with axis $\boldsymbol{u}$. The reconfiguration comes from that the rotation bar can be rotated along the groove of the ring base about the direction $\boldsymbol{n}$ which is the normal vector of the ring base plane Σ. This allows the revolute joint axis $\boldsymbol{u}$ to be alterable about $\boldsymbol{n}$ on the plane Σ and fixed along the groove. This changes the contribution of the rR joint in a parallel mechanism assembly and will make the mechanism reconfigurable.

The rR*PS* limb consisting of an rR joint, a prismatic joint and a spherical joint, is shown in Fig. 1(b). The function of an rR*PS* limb in a parallel mechanism is equivalent to a general *RPS* limb but with an additional reconfigurable rotation axis of the revolute joint.

Set a limb coordinate system ${}^1o{}^1x{}^1y{}^1z$ at the intersecting point of the rotation bar and the joint link on the plane Σ, where ${}^1x$ axis and ${}^1y$ axis are on the plane Σ while ${}^1z$ axis is along $\boldsymbol{n}$. The twist system of the rR*PS* limb is given as:

$$\left\{{}^1\boldsymbol{S}_1\right\}=\left\{\begin{array}{l}{}^1\boldsymbol{S}_{11}=\left[\boldsymbol{u}^{\mathrm{T}}\quad 0\times\boldsymbol{u}^{\mathrm{T}}\right]\\ {}^1\boldsymbol{S}_{12}=\left[0\quad \boldsymbol{s}^{\mathrm{T}}\right]\\ {}^1\boldsymbol{S}_{13}=\left[\boldsymbol{u}^{\mathrm{T}}\quad \boldsymbol{a}^{\mathrm{T}}\times\boldsymbol{u}^{\mathrm{T}}\right]\\ {}^1\boldsymbol{S}_{14}=\left[\boldsymbol{s}^{\mathrm{T}}\quad \boldsymbol{a}^{\mathrm{T}}\times\boldsymbol{s}^{\mathrm{T}}\right]\\ {}^1\boldsymbol{S}_{15}=\left[\boldsymbol{u}^{\mathrm{T}}\times\boldsymbol{s}^{\mathrm{T}}\quad \boldsymbol{a}^{\mathrm{T}}\times\left(\boldsymbol{u}^{\mathrm{T}}\times\boldsymbol{s}^{\mathrm{T}}\right)\right]\end{array}\right\} \tag{1}$$

where $(\bullet)^{\mathrm{T}}$ is the transpose of vector/matrix $(\bullet)$, $\boldsymbol{u}=(\cos\theta,\sin\theta,0)^{\mathrm{T}}$, $\boldsymbol{s}=(-\cos\alpha\sin\theta,\cos\alpha\cos\theta,\sin\alpha)^{\mathrm{T}}$ is the unit vector along the limb, $\boldsymbol{0}$ is a 1×3 zero vector and $\boldsymbol{a}$ is the position vector of the spherical center. In Eq. (1), the first twist is for the rR joint, the second is generated from the prismatic joint, and the last three are generated from the spherical joint. θ is the angle between the rotation bar ($\boldsymbol{u}$) and the ${}^1x$ axis, $\boldsymbol{\alpha}$ is the angle between the limb ($\boldsymbol{s}$) and its projection on plane ${}^1x{}^1o{}^1y$ (plane Σ). In the twist notation ${}^1\boldsymbol{S}_{ij}$, the first subscript i denotes the limb number, the second subscript j denotes the joint number within the limb and the leading superscript indicates the local frame.

The five twists in Eq. (1) form a five-system [45]. Thus, there is one reciprocal screw to Eq. (1) in the limb constraint system as

$$\left\{{}^1\boldsymbol{S}_1^r\right\}={}^1\boldsymbol{S}_1^r=[\boldsymbol{u}\quad \boldsymbol{a}\times\boldsymbol{u}]. \tag{2}$$

This gives a constraint force acting along a line passing through the spherical joint center with a direction parallel to the rotation axis ($\boldsymbol{u}$) of the rR joint. By altering the revolute joint axis $\boldsymbol{u}=(\cos\theta,\sin\theta,0)^{\mathrm{T}}$ with variable angle θ the constraint force in Eq. (2) is alterable and will change the constraint to the platform as analyzed in the following 3rR*PS* metamorphic parallel mechanism.

3. The 3rR*PS* metamorphic parallel mechanism and its reconfiguration

The 3rR*PS* metamorphic parallel mechanism as in Fig. 2 has three rR*PS* limbs symmetrically located on the base circle with radius r_b through the rR joints and on the platform circle with radius r_a through spherical joints. Let points A_i and B_i denote the spherical joint center and the rR joint center in limb i ($i=1,2,3$) respectively. $\boldsymbol{u}_i$ is the rotation axis of the rR joint in limb i. Locate a global coordinate system $oxyz$ at the geometric center o of the base with the negative part of y axis passing through rR joint center B_1 and z axis perpendicular to the base plane formed by $B_1B_2B_3$. Then, x axis is parallel to B_2B_3 as in Fig. 2. Based on symmetry, all the ring base plane Σ_i of the rR joint in limb i intersects the z axis with angle ϕ which is named rR joint base location angle. Let $\boldsymbol{a}_i$ and $\boldsymbol{b}_i$ denote the vectors of points A_i and B_i in the coordinate system $oxyz$, l_i be the limb length between the spherical joint center A_i and the rT joint center B_i. Similarly, a moving coordinate system $o'x'y'z'$ is attached at the platform center o' with the negative part of y' axis passing through spherical joint center A_1 and z' axis perpendicular to the platform plane formed by $A_1A_2A_3$.

Based on the above description, the geometric constraint of the 3rR*PS* is described in two parts. The first part expresses the length of the limbs

$$\left(\mathbf{R}\,\boldsymbol{a}_i'+\boldsymbol{p}-\boldsymbol{b}_i\right)^2=l_i^2\quad(i=1,2,3) \tag{3}$$

and the second part describes the constraint that each limb is perpendicular to the rotation axis $\boldsymbol{u}_i$ of the rR joint:

$$\left(\mathbf{R}\,\boldsymbol{a}_i'+\boldsymbol{p}-\boldsymbol{b}_i\right)^{\mathrm{T}}.\boldsymbol{u}_i=0\quad(i=1,2,3) \tag{4}$$

where $\mathbf{R}$ is the rotational matrix from the moving coordinate system to the global coordinate system $oxyz$, $\boldsymbol{p}=(p_x,p_y,p_z)^{\mathrm{T}}$ is the vector of the moving coordinate center o' expressed in the global coordinate system. $\boldsymbol{a}_i'$ is the position vector of spherical joint center A_i expressed in the moving coordinate system $o'x'y'z'$.

Please cite this article as: D. Gan, et al., Unified kinematics and optimal design of a 3rR*PS* metamorphic parallel mechanism with a reconfigurable revolute joint, Mech. Mach. Theory (2015), http://dx.doi.org/10.1016/j.mechmachtheory.2015.08.005

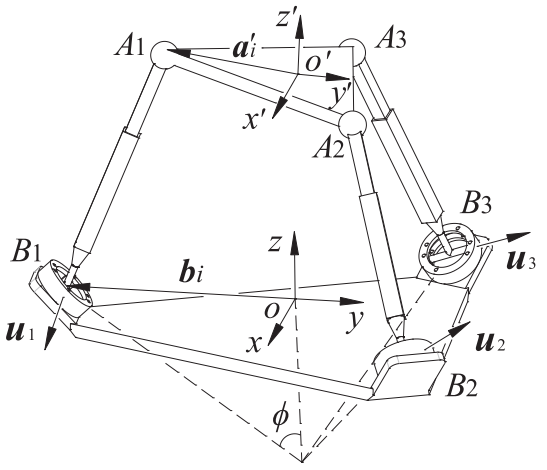

Fig. 2. The 3rR*PS* metamorphic parallel mechanism.

Based on the six constraint equations in Eqs. (3) and (4), the three independent rotation parameters in $\mathbf{R}$ and the three translation parameters in $\boldsymbol{p} = (p_x, p_y, p_z)^{\mathrm{T}}$ can be fully determined when l_i is given as actuation input of each prismatic joint. Thus, equations in Eq. (3) are related to the actuation and equations in Eq. (4) determine the mobility of the 3rR*PS* MPM. Based on the reconfiguration of the rR joint with variable $\boldsymbol{u}_i$ by rotating the ring base, the 3rR*PS* MPM is reconfigurable and can have the following different topologies with two different motion types.

Case 1. The three rR joint axis $\boldsymbol{u}_i$ are independent.

This is the general case as in Fig. 2, the position vector $\boldsymbol{p} = (p_x, p_y, p_z)^{\mathrm{T}}$ can be solved from the three equations in Eq. (4) as

$$\boldsymbol{p}^{\mathrm{T}} = \begin{bmatrix} (\mathbf{b}_1 - \mathbf{R}\,\boldsymbol{a}_1')^{\mathrm{T}}.\boldsymbol{u}_1 \\ (\mathbf{b}_2 - \mathbf{R}\,\boldsymbol{a}_2')^{\mathrm{T}}.\boldsymbol{u}_2 \\ (\mathbf{b}_3 - \mathbf{R}\,\boldsymbol{a}_3')^{\mathrm{T}}.\boldsymbol{u}_3 \end{bmatrix}^{\mathrm{T}} .[\,\boldsymbol{u}_1 \quad \boldsymbol{u}_2 \quad \boldsymbol{u}_3\,]^{-1}. \tag{5}$$

Thus, the translation parameters can be linearly solved for a given rotation matrix $\mathbf{R}$ but not inversely. Thus, considering kinematics simplicity, this topology is taken as pure rotation (3R) motion with parasitic translation motion that can be obtained from Eq. (5).

Before going to Case 2, the following *Cayley* formula [46] is introduced and will be used to describe the rotation between the moving coordinate system and the global coordinate system as matrix $\mathbf{R}$:

$$\mathbf{R} = \Delta^{-1}\begin{bmatrix} 1 + c_1^2 - c_2^2 - c_3^2 & 2(c_1c_2 - c_3) & 2(c_1c_3 + c_2) \\ 2(c_1c_2 + c_3) & 1 - c_1^2 + c_2^2 - c_3^2 & 2(c_2c_3 - c_1) \\ 2(c_1c_3 - c_2) & 2(c_2c_3 + c_1) & 1 - c_1^2 - c_2^2 + c_3^2 \end{bmatrix} \tag{6}$$

where $\Delta = 1 + c_1^2 + c_2^2 + c_3^2$, c_1, c_2 and c_3 are the Rodriguez–Hamilton parameters and $c_1 = k_x \tan(\gamma/2)$, $c_2 = k_y \tan(\gamma/2)$, $c_3 = k_z \tan(\gamma/2)$, which describes a 3D rotation about an axis $\boldsymbol{k}(kx, ky, kz)$ with angle γ.

Cayley formula uses the three independent Rodriguez–Hamilton parameters to represent 3D rotation motion and shows a big advantage in simplifying the following geometric constraint equations for mobility analysis and also on singularity and workspace representation in Section 5.

Case 2. The three rR joint axis $\boldsymbol{u}_i$ are dependent

Based on the symmetrical property, there are two dependent cases.

(1) Two $\boldsymbol{u}_i$ are dependent
This is the case when two $\boldsymbol{u}_i$ are parallel to each other and there are three cases ($\boldsymbol{u}_1 = \boldsymbol{u}_2$, $\boldsymbol{u}_1 = \boldsymbol{u}_3$, or $\boldsymbol{u}_2 = \boldsymbol{u}_3$). An example of $\boldsymbol{u}_1 = \boldsymbol{u}_3$ is in Fig. 3(a) and due to the symmetry $\boldsymbol{u}_1$, $\boldsymbol{u}_3$ should be parallel to the common line of the two base ring planes of the rR joints in limb 1 and limb 3. Then from Eq. (4) there is:

$$\begin{cases} \boldsymbol{p}^{\mathrm{T}}.\boldsymbol{u}_1 = (\boldsymbol{b}_1 - \mathbf{R}\,\boldsymbol{a}_1')^{\mathrm{T}}.\boldsymbol{u}_1 \\ \boldsymbol{p}^{\mathrm{T}}.\boldsymbol{u}_3 = (\boldsymbol{b}_3 - \mathbf{R}\,\boldsymbol{a}_3')^{\mathrm{T}}.\boldsymbol{u}_3 \\ 0 = (\boldsymbol{b}_1 - \boldsymbol{b}_2 - \mathbf{R}\,\boldsymbol{a}_1' + \mathbf{R}\,\boldsymbol{a}_2')^{T}.\boldsymbol{u}_1 \end{cases} \tag{7}$$

Please cite this article as: D. Gan, et al., Unified kinematics and optimal design of a 3rR*PS* metamorphic parallel mechanism with a reconfigurable revolute joint, Mech. Mach. Theory (2015), http://dx.doi.org/10.1016/j.mechmachtheory.2015.08.005

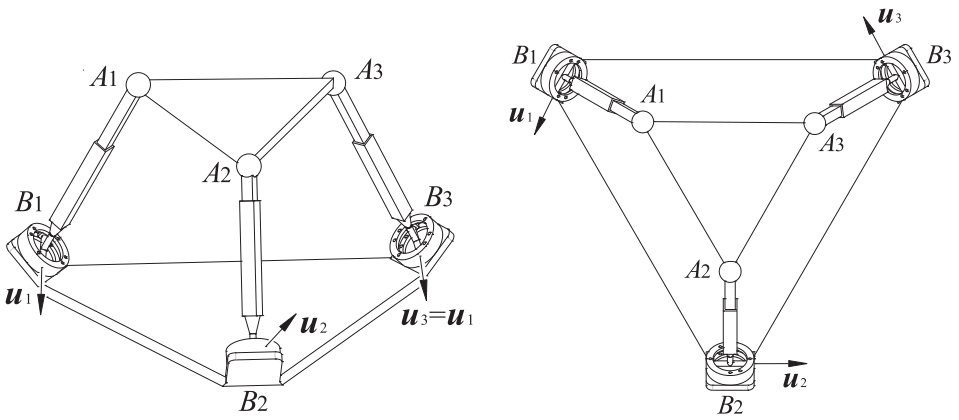

(a) $\boldsymbol{u}_1 = \boldsymbol{u}_3$ (b) $\boldsymbol{u}_1 + \boldsymbol{u}_2 + \boldsymbol{u}_3 = 0$

Fig. 3. Two topologies of the 3rR*PS* with 1T2R motion.

From Eq. (7) two of the three translation parameters (p_x, p_y, p_z) in $\boldsymbol{p}$ can be linearly solved from the first two equations while the third equation only relates to the rotation parameters in $\mathbf{R}$. By substituting *Cayley* formula from Eq. (6) into the third equation in Eq. (7), there is

$$c_3 = f\left(1, c_1, c_2, c_1^2, c_2^2\right) \tag{8}$$

where $f(\bullet)$ is a function of unknown power products in the bracket, with real constant coefficients depending on the input and mechanism dimensional parameters only. This further shows that the rotation about z axis can be linearly solved by the rotations about the other two axes. For simplicity, the mechanism is considered to have two main rotations about x axis and y axis. Thus, the mechanism has one translation and two rotation (1T2R) motion in this case.

(2) Three $\boldsymbol{u}_i$ are dependent

This is the case only when all the three $\boldsymbol{u}_i$ are on the base plane as in Fig. 3(b) where $\boldsymbol{u}_1 = (1, 0, 0)^{\mathrm{T}}$, $\boldsymbol{u}_2 = (-1/2, \sqrt{3}/2, 0)^{\mathrm{T}}$, $\boldsymbol{u}_3 = (-1/2, -\sqrt{3}/2, 0)^{\mathrm{T}}$, then $\boldsymbol{u}_1 + \boldsymbol{u}_2 + \boldsymbol{u}_3 = 0$, and there is

$$\begin{cases} \boldsymbol{p}^{\mathrm{T}}.\boldsymbol{u}_1 = (\boldsymbol{b}_1 - \mathbf{R}\,\boldsymbol{a}_1')^{\mathrm{T}}.\boldsymbol{u}_1 \\ \boldsymbol{p}^{\mathrm{T}}.\boldsymbol{u}_2 = (\boldsymbol{b}_2 - \mathbf{R}\,\boldsymbol{a}_2')^{\mathrm{T}}.\boldsymbol{u}_2 \\ 0 = (\boldsymbol{b}_1 - \mathbf{R}\,\boldsymbol{a}_1')^{\mathrm{T}}.\boldsymbol{u}_1 + (\boldsymbol{b}_2 - \mathbf{R}\,\boldsymbol{a}_2')^{\mathrm{T}}.\boldsymbol{u}_2 + (\boldsymbol{b}_3 - \mathbf{R}\,\boldsymbol{a}_3')^{\mathrm{T}}.\boldsymbol{u}_3. \end{cases} \tag{9}$$

Similar with Eq. (7), two of the three translation parameters (p_x, p_y, p_z) in $\boldsymbol{p}$ can be linearly solved from the first two equations while the third equation provides a constraint among the rotation parameters in $\mathbf{R}$. This can be further detailed as:

$$\begin{cases} p_x = (\boldsymbol{b}_1 - \mathbf{R}\,\boldsymbol{a}_1')^{\mathrm{T}}.\boldsymbol{u}_1 \\ p_y = (\boldsymbol{b}_1 - \mathbf{R}\,\boldsymbol{a}_1')^{\mathrm{T}}.\boldsymbol{u}_1 + 2(\boldsymbol{b}_2 - \mathbf{R}\,\boldsymbol{a}_2')^{\mathrm{T}}.\boldsymbol{u}_2/\sqrt{3} \\ c_3 = 0. \end{cases} \tag{10}$$

Thus translations along x axis and y axis can be linearly solved from the rotation motion while there is no rotation about z axis. The parallel mechanism in this case is considered to have one translation along the z axis and two rotations about x axis and y axis.

To summarize the above analysis, the 3rR*PS* MPM can have either pure rotation (3R) motion with parasitic translations or one translation and two rotation (1T2R) motion by reconfiguring the rotation axis of the rR joint into different directions. It should be noticed that there are infinite numbers of configurations with pure rotation motion by altering the rR joint in each limb as far as the three rotation axis vectors are not dependent. There are only four cases with 1T2R motion as stated in Case 2.

4. Unified kinematics modeling and analytical displacement analysis

The inverse displacement analysis of the 3rR*PS* metamorphic parallel mechanism is to obtain the actuation parameters (limb length l_i) based on the given platform position and orientation. When giving the platform position $\boldsymbol{p}$ (p_x, p_y, p_z) and orientation $\mathbf{R}$

Please cite this article as: D. Gan, et al., Unified kinematics and optimal design of a 3rR*PS* metamorphic parallel mechanism with a reconfigurable revolute joint, Mech. Mach. Theory (2015), http://dx.doi.org/10.1016/j.mechmachtheory.2015.08.005

described in the global coordinate system in Fig. 1, the actuation inputs which are the limb lengths can be calculated directly from Eq. (3):

$$l_i = \sqrt{(\mathbf{R}\,\boldsymbol{a}_i' + p - b_i)^2} \quad (i = 1, 2, 3). \tag{11}$$

This is the same for all the topologies with different mobility but it should be mentioned that, the platform position and orientation parameters cannot be given freely. They should follow the geometric constraint relations analyzed in Section 3 that the translations are calculated by given orientation for 3R motion case and two rotations and one translation can be given arbitrarily for the 1T2R motion case.

On contrary to the inverse one, forward displacement analysis is to solve the platform position $\boldsymbol{p}$ (p_x, p_y, p_z) and orientation $\mathbf{R}$ when giving the corresponding actuation parameters (l_i) for each topology. The strategy for the 3rR*PS* metamorphic parallel mechanism is to use the limb parameters to express the spherical joint center vector $\boldsymbol{a_i}$ to form the constraint equations based on the platform geometry. To do this, a limb coordinate system ${}^io{}^ix{}^iy{}^iz$ is attached to each rR joint as in Fig. 4, where ${}^iz$ axis is along the normal $\boldsymbol{n}$ of the base plane of the rR joint and ${}^iy$ axis intersects the z axis. The following solving procedure gives a unified forward kinematics analysis valid for all topologies of the 3rR*PS* MPM with different mobility.

Based on the above analysis and the coordinate systems of the 3rR*PS* MPM in Fig. 4, geometric constraints of the mechanism can be given as:

$$\begin{cases} \boldsymbol{b}_1 = (0, -r_b, 0)^T, \boldsymbol{b}_2 = r_b(\sin\pi/3, \cos\pi/3, 0)^{\mathrm{T}}, \boldsymbol{b}_3 = r_b(-\sin\pi/3, \cos\pi/3, 0)^{\mathrm{T}} \\ \boldsymbol{a}_1 = \boldsymbol{b}_1 + R_z(0)R_x(\phi - \pi/2)R_z(\theta_1)l_1(0, \cos\alpha_1, \sin\alpha_1) \\ \boldsymbol{a}_2 = \boldsymbol{b}_2 + R_z(2\pi/3)R_x(\phi - \pi/2)R_z(\theta_2)l_2(0, \cos\alpha_2, \sin\alpha_2) \\ \boldsymbol{a}_3 = \boldsymbol{b}_3 + R_z(4\pi/3)R_x(\phi - \pi/2)R_z(\theta_3)l_3(0, \cos\alpha_3, \sin\alpha_3) \end{cases} \tag{12}$$

where l_i is the length of limb i, $\mathbf{R}_k(g)$ represents a rotation about axis k with angle g and is used to translate the vector of the spherical joint center in the limb coordinate system to the global coordinate system in Fig. 4. θ_i describes the direction of the rR joint rotation axis $\boldsymbol{u}_i$ and α_i is the angle between the limb and its projection on the ${}^ix{}^io{}^iy$ plane (plane Σ) in limb i.

Based on this, the triangle of the platform geometry can be described as:

$$\begin{cases} \left(\sqrt{3}r_a\right)^2 = (\boldsymbol{a}_1 - \boldsymbol{a}_2)^2 \\ \left(\sqrt{3}r_a\right)^2 = (\boldsymbol{a}_1 - \boldsymbol{a}_3)^2 \\ \left(\sqrt{3}r_a\right)^2 = (\boldsymbol{a}_2 - \boldsymbol{a}_3)^2 \end{cases}. \tag{13}$$

Substituting Eq. (12) into Eq. (13) and applying $\cos\alpha_i = (1 - t_i^2)/(1 + t_i^2)$, $\sin\alpha_i = 2t_i/(1 + t_i^2)$, there is

$$\begin{cases} f_1\left(1, t_1, t_1^2, t_2^2, t_1t_2^2, t_1^2t_2^2\right) = 0 \\ f_2\left(1, t_3, t_3^2, t_1^2, t_3t_1^2, t_3^2t_1^2\right) = 0 \\ f_3\left(1, t_2, t_2^2, t_3^2, t_2t_3^2, t_2^2t_3^2\right) = 0 \end{cases} \tag{14}$$

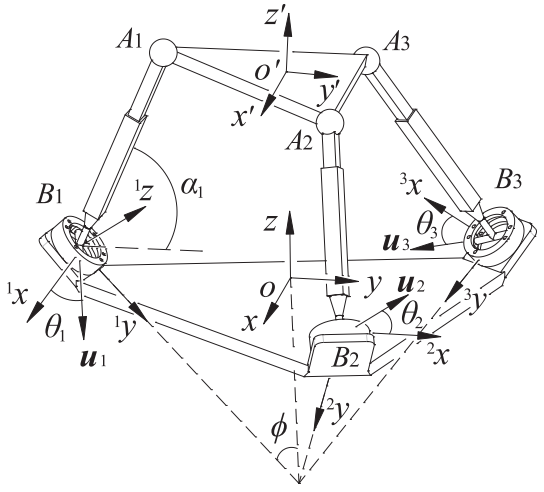

Fig. 4. Unified kinematics modeling of the 3rT*PS* with perpendicular constraint screws.

Please cite this article as: D. Gan, et al., Unified kinematics and optimal design of a 3rR*PS* metamorphic parallel mechanism with a reconfigurable revolute joint, Mech. Mach. Theory (2015), http://dx.doi.org/10.1016/j.mechmachtheory.2015.08.005

where $f_i(\bullet)$ is a linear function of the power products in the bracket with coefficients depending on known parameters only, t_i represents $\mathrm{Tan}(\alpha_i/2)$.

By using Sylvester's dialytic elimination method [32] for the first two equations in Eq. (14), there is

$$f_4\left(1, t_3, t_2^2, t_3^2, t_2^2 t_3, t_3^3, t_2^4, t_3^4, t_2^2 t_3^2, t_2^2 t_3^3, t_2^4 t_3^1, t_2^2 t_3^4, t_2^4 t_3^2, t_2^4 t_3^3, t_2^4 t_3^4\right) = 0 \tag{15}$$

where $f_4(\bullet)$ is a linear function of the power product in the bracket with coefficients depending on known parameters only.

Then, following the same method for Eq. (15) and the third equation in Eq. (14), a polynomial with only unknown t_3 can be obtained as:

$$\sum_{i=0}^{+16} h_i t_3^i = 0 \tag{16}$$

where coefficient h_i are the real constants depending on input data only.

This shows that a univariate equation in t_3 of degree 16 is obtained.

Solving Eq. (16), sixteen solutions of t_3 can be obtained. Then, t_2 can be solved by substituting each solution of t_3 into the third equation in Eq. (14) and selecting the roots satisfying Eq. (15). Following this, t_1 can be solved by substituting each pair of solutions of t_2 and t_3 into the first equation in Eq. (14) with proof of the second equation in Eq. (14). Based on this, sixteen pair of solutions of t_1, t_2, t_3 are obtained and the spherical joint center A_i can be calculated by substituting $\alpha_i = 2\mathrm{ArcTan}(t_i)$ into Eq. (12). Then, the platform position and orientation can be determined using the three spherical joint centers with Fig. 4 as:

$$\begin{cases} \boldsymbol{z}' = (\boldsymbol{a}_2 - \boldsymbol{a}_1) \times (\boldsymbol{a}_3 - \boldsymbol{a}_1) / \|(\boldsymbol{a}_2 - \boldsymbol{a}_1) \times (\boldsymbol{a}_3 - \boldsymbol{a}_1)\| \\ x' = (\mathbf{a}_2 - \mathbf{a}_3) / \left(\sqrt{3} r_a\right) \\ \boldsymbol{y}' = \boldsymbol{z}' \times \boldsymbol{x}' \\ R = (\boldsymbol{x}', \boldsymbol{y}', \boldsymbol{z}') \\ \boldsymbol{p} = \boldsymbol{a}_1 + r_a \boldsymbol{y}'. \end{cases} \tag{17}$$

This shows the unified forward kinematics solution of the 3rR*PS* metamorphic parallel mechanism for both the 3R motion and the 1T2R motion.

5. Singularity loci and singularity-free workspace

5.1. Singularity loci based on Jacobian matrix with reciprocal screws

The infinitesimal twist [47] of the moving platform of the 3rR*PS* MPM can be written as the linear combination of instantaneous twists of each limb:

$$\boldsymbol{S}_G = \dot{\phi}_{i1} \boldsymbol{S}_{i1} + \dot{l}_i \boldsymbol{S}_{i2} + \dot{\phi}_{i3} \boldsymbol{S}_{i3} + \dot{\phi}_{i4} \boldsymbol{S}_{i4} + \dot{\phi}_{i5} \boldsymbol{S}_{i5} \qquad (i = 1, 2, 3) \tag{18}$$

where $\boldsymbol{S}_G$ represents the infinitesimal twist of the moving platform, $\boldsymbol{S}_{ij}$ ($j = 1,2,3,4,5$) denotes the unit screw of the jth 1-DOF joint in limb i, $\dot{l}_i$ is the distance rate of the prismatic joint in limb i, $\dot{\phi}_{ij}$ ($j = 1,3,4,5$) represents the angular rate of the rR joint and spherical joint in limb i.

By locking the active joints in the limbs temporarily and taking reciprocal product on both sides of (18), there is

$$\begin{bmatrix} \boldsymbol{S}_{i1}^r & \boldsymbol{S}_{i2}^r \end{bmatrix}^{\mathrm{T}} \circ \boldsymbol{S}_G = \begin{bmatrix} 0 & \dot{l}_i \end{bmatrix}^{\mathrm{T}} \quad (i = 1, 2, 3) \tag{19}$$

where $\boldsymbol{S}_{i1}^r$ is the reciprocal screw of geometric constraint to all motion screws in limb i and it passes through the spherical joint center with direction parallel to rotation axis $\boldsymbol{u}_i$ of the rR joint as in Eq. (2). $\boldsymbol{S}_{i2}^r$ is the actuation screw reciprocal to all motion screws in Eq. (18) except the prismatic joint screw $\boldsymbol{S}_{i2}$ and it is collinear with the limb.

Equations in Eq. (19) for the three limbs can be rewritten in matrix form as:

$$\begin{bmatrix} \boldsymbol{S}_{11}^r \\ \boldsymbol{S}_{21}^r \\ \boldsymbol{S}_{31}^r \\ \boldsymbol{S}_{12}^r \\ \boldsymbol{S}_{22}^r \\ \boldsymbol{S}_{32}^r \end{bmatrix} \circ \boldsymbol{S}_G = \mathbf{J} \boldsymbol{S}_G = \begin{bmatrix} \boldsymbol{a}_1 \times \boldsymbol{u}_1 & \boldsymbol{u}_1 \\ \boldsymbol{a}_2 \times \boldsymbol{u}_2 & \boldsymbol{u}_2 \\ \boldsymbol{a}_3 \times \boldsymbol{u}_3 & \boldsymbol{u}_3 \\ \boldsymbol{b}_1 \times \boldsymbol{s}_1 & \boldsymbol{s}_1 \\ \boldsymbol{b}_2 \times \boldsymbol{s}_2 & \boldsymbol{s}_2 \\ \boldsymbol{b}_3 \times \boldsymbol{s}_3 & \boldsymbol{s}_3 \end{bmatrix} \mathbf{S}_G = \begin{bmatrix} 0 \\ 0 \\ 0 \\ \dot{l}_1 \\ \dot{l}_2 \\ \dot{l}_3 \end{bmatrix}. \tag{20}$$

In Eq. (20), $\mathbf{J}$ is the 6 by 6 Jacobian matrix which maps velocities between the manipulator and the actuation input. Once the manipulator meets singular configurations, this mapping loses its function and the rank of the Jacobian matrix decreases to be less than 6.

Please cite this article as: D. Gan, et al., Unified kinematics and optimal design of a 3rR*PS* metamorphic parallel mechanism with a reconfigurable revolute joint, Mech. Mach. Theory (2015), http://dx.doi.org/10.1016/j.mechmachtheory.2015.08.005

This can be also interpreted that the six constraint forces in **J** are linearly dependent. Inversely, identifying the dependent conditions for the constraint forces in the workspace will reveal the singular configurations of the manipulator. In order to demonstrate this, some dimensionless parameters with physical constraints are given as: the platform radius $r_a = 1$, base radius $r_b = 2$, $\phi = \pi/2 - \mathrm{ArcSin}(\sqrt{3}/3)$ representing that the three normal vectors of the three rR joints are perpendicular to each other.

Type 2 singularities appear when the determinant of **J** equals to zero. Based on the rotation matrix **R** in (6) and mobility analysis in Section 3, the determinant of **J** is given by:

$$|\mathbf{J}| = \begin{cases} f_5(c_1, c_2, c_3, \ldots) & 3R \text{ motion} \\ f_6(c_1, c_2, p_z, \ldots) & 1T2R \text{ motion} \end{cases} \tag{21}$$

where f_5 is a function of c_1, c_2 and c_3 with their products up to 10th order for the topologies with 3R motion and f_6 is a function of c_1, c_2 and p_z with their products up to 11th order for the topologies with 1T2R motion. Those parameters are used respectively to represent the singularity points of the platform. By equalling Eq. (21) to zero, all singular points can be found and some examples are illustrated in Figs. 5 and 6.

In Fig. 5, the singularity loci of the 3rR*PS* MPM with 1T2R motion ($\theta_1 = \theta_2 = \theta_3 = 0$) is shown. It can be seen that the loci is symmetrical due to the symmetrical limb arrangement. Two singular configurations and their corresponding points on the singularity loci are shown in Fig. 5. It agrees with the conclusion [48] that in singularity configurations the four planes, the platform plane and a plane from each limb formed by the actuation force and constraint force in the limb, intersect at one point which makes the rank of the Jacobian matrix 5. It can be also found that when p_z is close to zero which is that the platform is close to the base, there are more possibilities to meet singularity configurations. However, in real applications, the platform will work with positive p_z much bigger than zero for which the singularity loci is quite uniform and represented by the tetrahedron shaped surface with an open side along the z direction and a vertex at the zero point with $c_1 = c_2 = p_z = 0$ as in Fig. 5.

As analyzed in Section 3, there are various topologies of the 3rR*PS* MPM with 3R motion by changing the rR joint rotation axes to different directions. The following shows singularity loci of four cases in Fig. 6. It can be seen that when $\theta_1 = \theta_2 = \theta_3$ the singularity loci are symmetrical due to the symmetrical limb arrangement. The case with $\theta_1 = \theta_2 = \theta_3 = \pi/2$ gives similar spherical parallel mechanism to the pyramid parallel mechanism [49]. When the three rR joint axes do not have the same angle θ, the loci is not symmetrical as shown in Fig. 6(b). Generally, the space close to the center ($c_1 = c_2 = c_3 = 0$) is separated into upper and lower part by the loci which are the main singularities in the mechanism workspace as shown in the following section.

5.2. Singularity-free workspace

In the 3rR*PS* MPM, each limb length has two limits (lower and upper) which constrain the actuation range and determine the workspace of the platform. Thus, the platform workspace boundaries can be expressed by the two limits $l_{\mathrm{imax/min}}$ following the geometric constraints in Eqs. (3) and (4):

$$\left(\mathbf{R}\,\boldsymbol{a}_i' + \boldsymbol{p} - \boldsymbol{b}_i\right)^2 = l_{i\,\mathrm{max/min}}^2 \quad (i = 1, 2, 3). \tag{22}$$

Similar to the singularity representation, the independent parameters are used to illustrate the boundary with (c_1, c_2, c_3) for the 3R motion and (c_1, c_2, p_z) for the 1T2R motion. Two examples are shown in Fig. 7(a) and (b) in which the following parameters are used: spherical joint rotation angle ≤ π/3 rad, rR joint rotation angle ≤ π/3 rad, limb length $1.6 \le l_i \le 2.88$.

Fig. 7(a) shows that workspace of the 1T2R case only exists in the area with p_z between 1 and 3 based on the geometric parameters and constraints given. Most of the part is singularity-free as seen in the combination figure with the singularity loci in Fig. 7(a). Differently, workspace of the 3R case has symmetrical parts with respect to the plane $c_3 = 0$ as in Fig. 7(b) and they are corresponding to positive and negative rotations about *z* axis. Comparing with the singularity loci, the workspace is separated into two singularity-

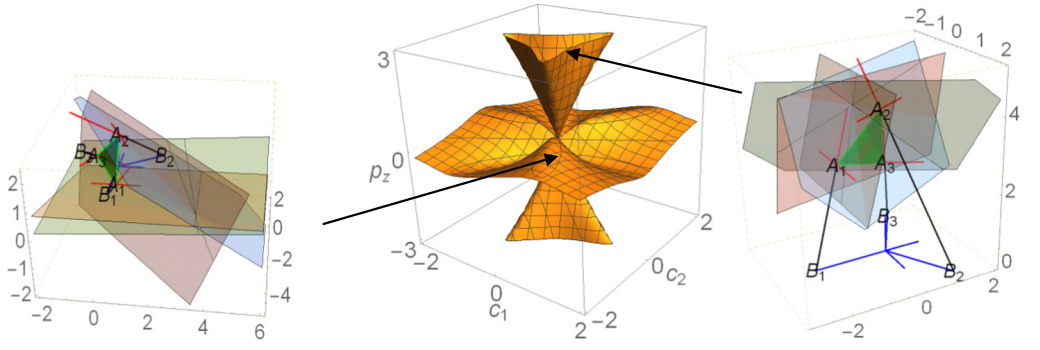

(c_1=0.5, c_2=–0.5, p_z=0.3) (c_1=0.2, c_2=–0.79, p_z=3)

Fig. 5. Singularity loci and two singular configurations of the 1T2R case ($\theta_1 = \theta_2 = \theta_3 = 0$).

Please cite this article as: D. Gan, et al., Unified kinematics and optimal design of a 3rR*PS* metamorphic parallel mechanism with a reconfigurable revolute joint, Mech. Mach. Theory (2015), http://dx.doi.org/10.1016/j.mechmachtheory.2015.08.005

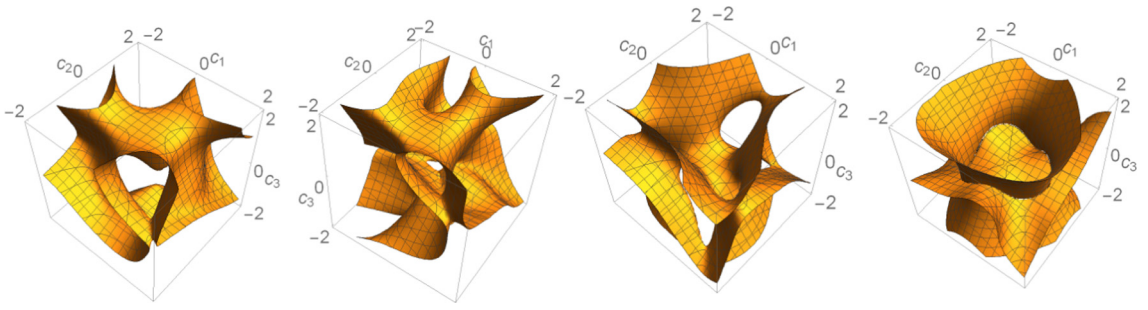

(a) $\theta_1 = \theta_2 = \theta_3 = \pi/6$ (b) θ_1=0, $\theta_2 = \pi/6$, $\theta_3 = \pi/4$ (c) $\theta_1 = \theta_2 = \theta_3 = \pi/3$ (d) $\theta_1 = \theta_2 = \theta_3 = \pi/2$

Fig. 6. Singularity loci of topologies with 3R motion.

free parts. To avoid singularities, the mechanism needs to work with positive or negative *z*-axis rotation only. The way to define singularity-free workspace in this section will be used as in the optimal design in the following section.

6. Parameter effect on maximum singularity-free workspace

Singularity-free workspace can be taken as the primary performance index for a parallel mechanism and is an important topic in mechanism design. This section aims at exploring effect of some key parameters of the 3rR*PS* MPM on its singularity-free workspace. Each topology of the 3rR*PS* MPM is a parallel mechanism and to show the effect by covering all working topologies with different motion types is a challenge. In the following, the two main topologies with 1T2R motion ($\theta_1 = \theta_2 = \theta_3 = 0$) and 3R motion ($\theta_1 = \theta_2 = \theta_3 = \pi/2$) will be considered together.

Based on the kinematics model shown in Fig. 4, key parameters of the 3rR*PS* MPM are the base and platform sizes (r_b and r_a), rR joint base location angle ϕ and the limb length range ($l_{min} \le l_i \le l_{max}$) which is the same for all three limbs. Mechanical constraints including maximum passive joint angles and limb interference should also be considered in the calculation. In the following, passive joint angles are limited in the range as $-\psi_{max} \le \psi_i \le \psi_{max}$, where ψ_i denotes rotation angle from its home position of any revolute joint, and spherical joint along three orthogonal directions one of which is along the limb at the home position. ψ_{max} is given π/3 in this paper. The minimum distance between any two limbs is limited to be 0.01 to avoid limb interference.

In the following, effect of the key parameters (r_a, r_b, ϕ, l_i) on maximum singularity-free workspace *V* will be illustrated for the two topologies with 1T2R motion ($\theta_1 = \theta_2 = \theta_3 = 0$) and 3R motion ($\theta_1 = \theta_2 = \theta_3 = \pi/2$). *V* is calculated as the volume inside of the workspace boundaries and the singularity surface as demonstrated in Section 5.2.

(1) Effect of limb length range ($l_{min} \le l_i \le l_{max}$).
Based on the kinematics, it can be imagined that limb length range limits the translation along *z* axis of the 1T2R motion and both of them can be as large as infinite. But this is different for the 3R motion with parasitic translation motion with which the limb length has minimum and maximum values even if there is no other constraint. This is the reason that limb length range is selected as one of the parameters for optimization as an arbitrarily selected limb length range may not cover the effective workspace of the 3R motion. By using dimensionless values $r_a = 1$, $r_b = 2$, $l_{max} = 1.8 l_{min}$, workspace volume *V* with respect to different l_{min} (from 1.3 to 4) under different rR joint base location angle ϕ for the two topologies are shown in Fig. 8. In Fig. 8(a), it can be seen that the workspace volume of the 3R motion has a peak value for each angle ϕ while the minimum limb length l_{min} corresponding to the peak value increases when ϕ increases from 50° to 80°. The peak value is bigger when the angle ϕ is larger indicating that a larger rR joint base location angle ϕ can help increase the workspace of the 3R motion when a corresponding limb length l_{min} is provided. An example of the peak workspace volume *V* of the 3R motion is shown

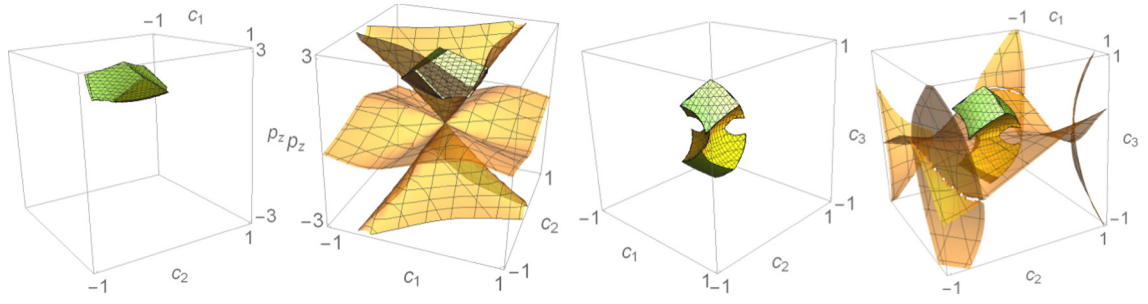

(a) 1T2R motion ($\theta_1 = \theta_2 = \theta_3 = 0$) (b) 3R motion ($\theta_1 = \theta_2 = \theta_3 = \pi/3$)

Fig. 7. Workspace of different topologies.

Please cite this article as: D. Gan, et al., Unified kinematics and optimal design of a 3rR*PS* metamorphic parallel mechanism with a reconfigurable revolute joint, Mech. Mach. Theory (2015), http://dx.doi.org/10.1016/j.mechmachtheory.2015.08.005

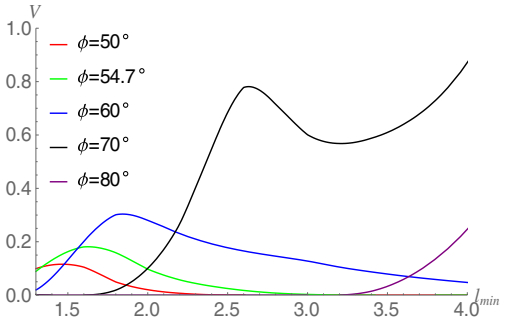

(a) 3R motion V vs l_{min}

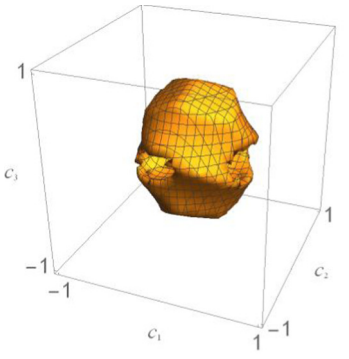

(b) 3R with ϕ=70° and l_{min}=2.8

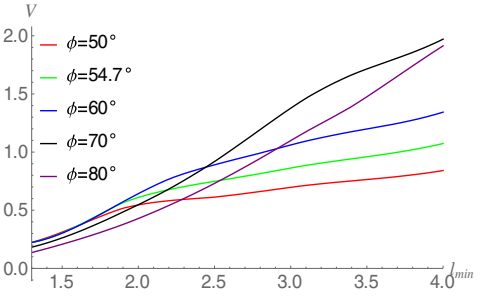

(c) 1T2R motion V vs l_{min}

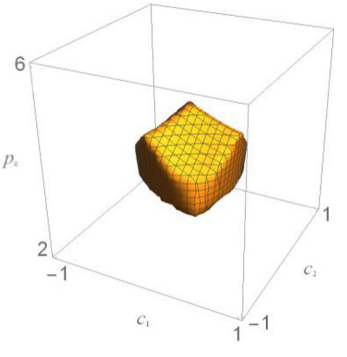

(d) 1T2R with ϕ=70° and l_{min}=2.8

Fig. 8. Maximum singularity-free workspace volume and the limb length range.

in Fig. 8(b) which shows the boundary is symmetrical due to the symmetrical limb arrangement. The maximum rotation about z axis is around $\pm 68°$ ($c_3 = \pm 0.675$), around $\pm 58°$ ($c_1 = c_2 = \pm 0.56$) about x axis and y axis.

Fig. 8(c) shows the workspace volume of the 3r*RPS* MPM with 1T2R motion with respect to the same limb length range ($l_{\min}$ from 1.3 to 4) and variable rR joint base location angle ϕ. There is a clear trend that the workspace volume increases when the minimum limb length $l_{\min}$ increases. A bigger angle ϕ provides larger V when ϕ is less than 70° and $l_{\min}$ is over 2.5 while the workspace volume decreases when ϕ is 80° (purple line). Thus to have a good workspace volume, a longer $l_{\min}$ and an angle ϕ close to 70° will be good design values. An example of the workspace volume V of the 1T2R motion is shown in Fig. 8(d) which shows the boundary is also symmetrical. The maximum translation along z axis is around 2.1($2.72 \le p_z \le 4.82$), with rotation angle $-60.6°$ to 52.7° ($-0.585 \le c_1 \le 0.496$) about x axis and $\pm 58°$ ($c_2 = \pm 0.53$) about y axis.

Thus, considering the two topologies and the workspace volume curves in Fig. 8, a longer $l_{\min}$ and a larger angle ϕ close to 70° are good design values.

(2) Effect of the base radius r_b.

By using $r_a = 1$, $l_{\max} = 1.8 l_{\min}$, $l_{\min} = 3.1$, the maximum singularity-free workspace volumes with respect to different base radius r_b (from 0.7 to 4.5) and different rR joint base location angle ϕ are shown in Fig. 9 for the 3R and 1T2R motion. The general trend is similar for both cases that the peak value of the workspace volume is around the same value for different ϕ and it requires smaller base size r_b when angle ϕ is bigger to reach the peak volume V. It can also be seen that a similar base size r_b can make both topologies reach the maximum singularity-free workspace volume for a given angle ϕ. For example, $r_b \approx 2.9$ gives the maximum $V \approx 0.85$ for the 3R motion with $\phi = 60°$ (blue curve) in Fig. 9(a) while $r_b \approx 3$ gives the maximum $V \approx 1.6$ for the 1T2R motion with same $\phi = 60°$ (blue curve) in Fig. 9(b). This makes it easy to select base size r_b by giving rR joint base location angle ϕ or inversely.

(3) Effect of the platform radius r_a.

By selecting $r_b = 2$, $l_{\max} = 1.8 l_{\min}$, $l_{\min} = 3.1$, the maximum singularity-free workspace volume with respect to different base radius r_a (from 0.3 to 4.1) and different rR joint base location angle ϕ are shown in Fig. 10 for the 3R and 1T2R motion. Generally, a smaller platform size r_b will provide larger workspace volume V for both cases. The increase of angle ϕ will increase the volume V a lot in 3R motion when ϕ is less than 70° as in Fig. 10(a) and it drops a lot for $\phi = 80°$ while V is almost zero when $\phi = 50°$. The trend is similar for the 1T2R motion in Fig. 10(b) but angle ϕ does not affect the workspace volume V as much as that in the 3R case. Thus, a smaller platform size r_a and a larger angle ϕ close to 70° are preferable.

Please cite this article as: D. Gan, et al., Unified kinematics and optimal design of a 3r*RPS* metamorphic parallel mechanism with a reconfigurable revolute joint, Mech. Mach. Theory (2015), http://dx.doi.org/10.1016/j.mechmachtheory.2015.08.005

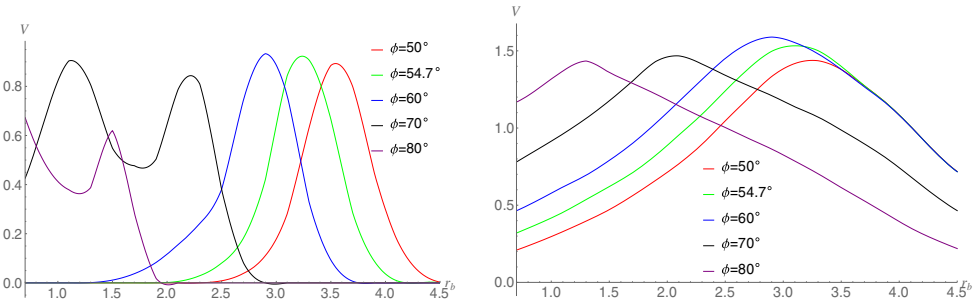

(a) 3R motion V vs r_b (b) 1T2R motion V vs r_b

Fig. 9. Maximum singularity-free workspace volume and the base radius r_b.

The above gives a general idea of the effect of those key parameters on the maximum singularity-free workspace of both 3R and 1T2R motion of the 3r*RPS* MPM. This provides references at the initial stage of the mechanism design. In the following, a systematic way will be shown on the optimal design considering both workspace and kinematics performance.

7. Optimal design of the 3r*RPS* MPM

As mentioned in Section 6, each topology of the 3r*RPS* MPM is a parallel mechanism and there is an optimal design for it based on selected design criteria. To have an optimal design of the metamorphic parallel mechanism to cover all working topologies with different motion types is very challenge and time consuming. In this section, the two main topologies of 1T2R motion ($\theta_1 = \theta_2 = \theta_3 = 0$) and 3R motion ($\theta_1 = \theta_2 = \theta_3 = \pi/2$) will be considered together in the optimal design which gives the best combined performance for both topologies.

7.1. Design variables and performance indices

As discussed in Section 6, key parameters of the 3r*RPS* MPM in the optimization are the base and platform sizes (r_b and r_a), rR joint base location angle ϕ and the limb length range ($l_{\min} \le l_i \le l_{\max}$). Considering practical mechanical limb strokes, it is commonly $l_{\max} = 1.8 l_{\min}$ which means the stroke of the limb can be eighty percent of its minimum length. Then $l_{\min}$ will be taken as one of the key parameters in the design. To have a relative relation, the length parameters are normalized by the base size r_b as $\lambda_a = r_a/r_b$, $\lambda_{lmin} = l_{\min}/r_b$. Thus, λ_a represents the ratio between the platform and base sizes and λ_{lmin} shows the ratio of the minimum limb length over the base size.

In addition to the maximum singularity-free workspace, kinematics performance of the parallel mechanism will be another objective in the optimal design. For the kinematics performance, condition number $k_i = \sigma_{\max}/\sigma_{\min}$, ($\sigma_{\max}$ and $\sigma_{\min}$ are the maximum and minimum singular values of the Jacobian matrix) is a widely used parameter in parallel mechanism design and optimization [50]. For the 3R topology, the Jacobian matrix has unified unit of rotation angles as in Eq. (A5) in the Appendix A. However, the 1T2R topology has coupled translation and rotation due to which the Jacobian matrix has mixed units which causes inconsistent condition numbers in representing kinematics performance. In this paper, the condition number is calculated using the dimensional homogeneous Jacobian matrix [51] which is derived in the Appendix A.

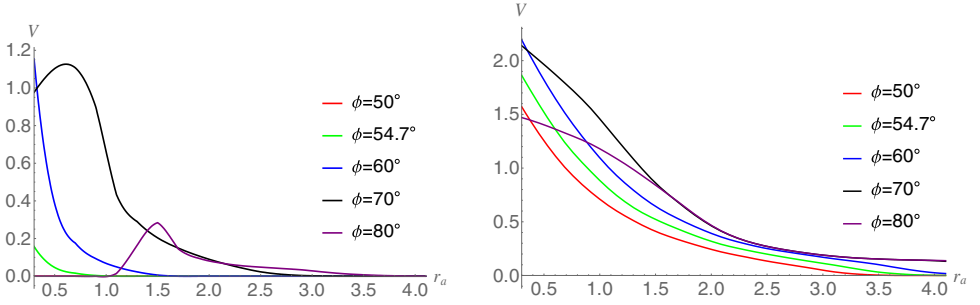

(a) 3R motion V vs r_a (b) 1T2R motion V vs r_a

Fig. 10. Maximum singularity-free workspace volume and the base radius r_a.

Please cite this article as: D. Gan, et al., Unified kinematics and optimal design of a 3r*RPS* metamorphic parallel mechanism with a reconfigurable revolute joint, Mech. Mach. Theory (2015), http://dx.doi.org/10.1016/j.mechmachtheory.2015.08.005

Optimal design of the 3rR*PS* MPM in this paper is to find the best parameter set to have maximum singularity-free workspace with good kinematics performance covering the two topologies of 1T2R motion ($\theta_1 = \theta_2 = \theta_3 = 0$) and 3R motion ($\theta_1 = \theta_2 = \theta_3 = \pi/2$). Thus, the optimal design cost function can be given as:

$$\begin{cases} \text{maximize} & V \\ \text{maximize} & k \end{cases}, \qquad k = \frac{V}{\int_V k_i dV} \tag{23}$$

Subject to: $-\pi/3 \le \psi_i \le \pi/3$,

$0.3 \le \lambda_a \le 1$,
$0.5 \le \lambda_{l\min} \le 1.6$,
$40^\circ \le \phi \le 80^\circ$,
limb distance ≤ 0.01,

where V is the maximum singularity-free workspace volume, k is the inverse average condition number in the workspace V and is between 0 and 1. The best kinematics performance corresponds to the value 1 when the velocity mapping is isotropic.

7.2. Optimal design

Based on the optimal design function in Eq. (23), the combined effect of the key parameters on the maximum singularity-free workspace and kinematics performance has been calculated and the results are illustrated in Fig. 11 for both 3R and 1T2R topologies. In general, a larger singularity-free workspace corresponds to a worse average kinematics performance. A smaller platform size (λ_a) gives a larger singularity-free workspace for both topologies as shown in Fig. 11(a) and (c) in which the blue one ($\lambda_a = 0.3$) shows the best and the red one ($\lambda_a = 1$) is the worst. This is directly opposite to the kinematics performance as in Fig. 11(b) and (d) in which the red ones provide higher numbers while the blue ones are at the bottom.

For the 3R topology, an approximate ratio $\lambda_{lmin}/\phi = 1$ between the minimum leg length and rR joint base location angle ϕ will give a large workspace for a given platform size as shown by the bump parts of each color in Fig. 11(a). The maximum singularity-free

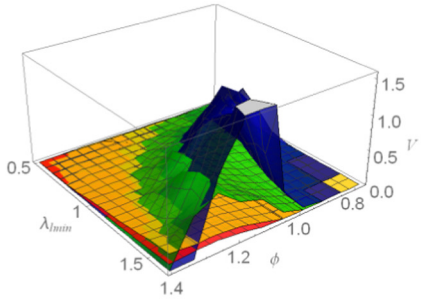

(a) 3R workspace

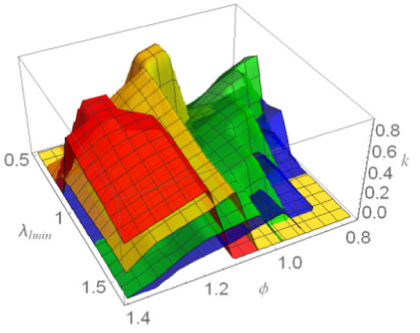

(b) 3R kinematics performance

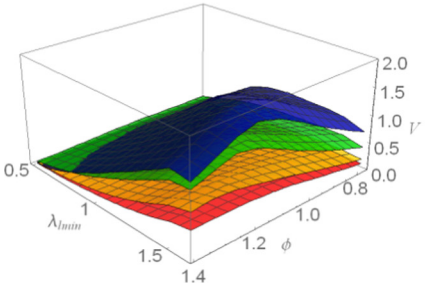

(c) 1T2R workspace

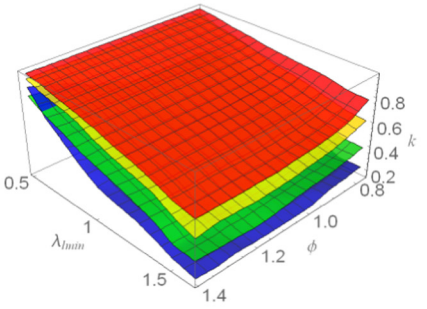

(d) 1T2R kinematics performance

Fig. 11. Optimal design of the 3rR*PS* MPM (blue for $\lambda_a = 0.3$, green for $\lambda_a = 0.5$, yellow for $\lambda_a = 0.8$, red for $\lambda_a = 1$). (For interpretation of the references to color in this figure legend, the reader is referred to the web version of this article.)

Please cite this article as: D. Gan, et al., Unified kinematics and optimal design of a 3rR*PS* metamorphic parallel mechanism with a reconfigurable revolute joint, Mech. Mach. Theory (2015), http://dx.doi.org/10.1016/j.mechmachtheory.2015.08.005

workspace increases when λ_{lmin} and ϕ increase at the same time. The largest workspace is represented by the point on the blue surface ($\lambda_a = 0.3$) with $\lambda_{lmin} = 1.6$, $\phi = 64°$. For each platform size, it can be also found that when the limb length is not enough, the workspace is zero. This happens for a small ϕ with a large λ_{lmin} or a big ϕ with a small λ_{lmin}. As mentioned above, the kinematics performance has an opposite trend with workspace as in Fig. 11(b). For a fixed platform size, the average condition number increases when both λ_{lmin} and ϕ decrease at the same time. The best kinematics performance is represented by the peak point on the yellow surface ($\lambda_a = 0.8$) with $\lambda_{lmin} = 0.8$, $\phi = 60°$.

For the 1T2R topology, surfaces of both workspace and kinematics performance are smoother than the 3R case as in Fig. 11(c) and (d). The trend is also clear that when the minimum leg length λ_{lmin} increases, the maximum singularity-free workspace increases while the average condition number decreases. A smaller rR joint base location angle ϕ is preferable considering the kinematics performance while a specific value (around $\phi = 70°$) provides the largest singularity-free workspace for a fixed platform size (λ_a).

To conclude the above optimal design results, a larger angle ϕ close to 70°, a bigger minimum limb length l_{min}, a smaller platform size r_a will provide the best set of parameters to have a maximum singularity-free workspace for both 3R and 1T2R motion of the 3rR*PS* MPM. However, the kinematics performance represented by the average condition number of the Jacobian matrix has an opposite trend. A smaller ϕ, smaller minimum limb length l_{min}, and a bigger platform size r_a will provide better average kinematics performance. A trade-off needs to be made between the two performance objectives and also between the two topologies which share the same mechanical parameters. A combined criterion can be given as

$$\text{maximize} \quad C = w_1(w_{11}V_{3R} + w_{12}k_{3R}) + w_2(w_{21}V_{1T2R} + w_{22}k_{1T2R}) \tag{24}$$

where w_1 and w_2 are the weights of the 3R topology and the 1T2R topology in the objective function with $w_1 + w_2 = 1$, $0 \le w_1, w_2 \le 1$, w_{i1} and w_{i2} ($i = 1$ for 3R, $i = 2$ for 1T2R) are the weights for maximum singularity-free workspace and kinematics performance of each topology with $w_{i1} + w_{i2} = 1$, $0 \le w_{i1}$, and $w_{i2} \le 1$. V_{3R} and V_{1T2R} are the normalized workspace and $0 \le V_{3R}, V_{1T2R} \le 1$. As mentioned above, the inverse averaged condition numbers k_{3R} and k_{1T2R} follow $0 \le k_{3R}, k_{1T2R} \le 1$.

An example can be given as $w_1 = 0.4$, $w_2 = 0.6$, $w_{11} = 0.5$, $w_{12} = 0.5$, $w_{21} = 0.7$, $w_{22} = 0.3$, which means the performance of the 3R topology weighs forty percent and the 1T2R topology contributes sixty percent to the overall objective. For the 3R topology, workspace and kinematics performance have equal weight while workspace shows more important with seventy percent in the 1T2R topology optimization. Based on those, the best performance is found at $C = 0.637$, with $\lambda_a = 0.3$, $\lambda_{lmin} = 1.6$, and $\phi = 64°$, which is on the blue surface in Fig. 11. This shows that the workspace dominates the result. If changing weights of the workspace to be $w_{11} = 0.3$, $w_{12} = 0.7$, $w_{21} = 0.5$, $w_{22} = 0.5$, the result will be $C = 0.534$, with $\lambda_a = 0.8$, $\lambda_{lmin} = 0.6$, and $\phi = 60°$, which corresponds to a point on the yellow surface in Fig. 11. Thus, priorities represented by the function weights can be given to the topologies and their workspace or kinematics performance in the optimization. Then Eq. (24) will give the optimal result with the best combined performance.

8. Reconfiguration strategy and mechanism design

Reconfiguration of the 3rR*PS* metamorphic parallel mechanism comes from reconfiguration of its rR joint. Thus the rR joint tuning is a key step in the configuration change between the 3R and 1T2R motion. One solution is proposed as illustrated in Fig. 12 and a worm gear system is used for the rR joint tuning. A prototype of the rR joint is shown in Fig. 12(a) in which the rotation bar is attached with the worm wheel which can be rotated with respect to the base ring by the worm which realizes the alteration of the rR joint axis $\boldsymbol{u}$ and the axis can be fixed by locking the worm control. A small motor can be attached to the worm in each rR joint to tune the rR joint axis in the 3rR*PS* MPM as in Fig. 12(b). A home position for each limb can be defined as a configuration that the limb axis is

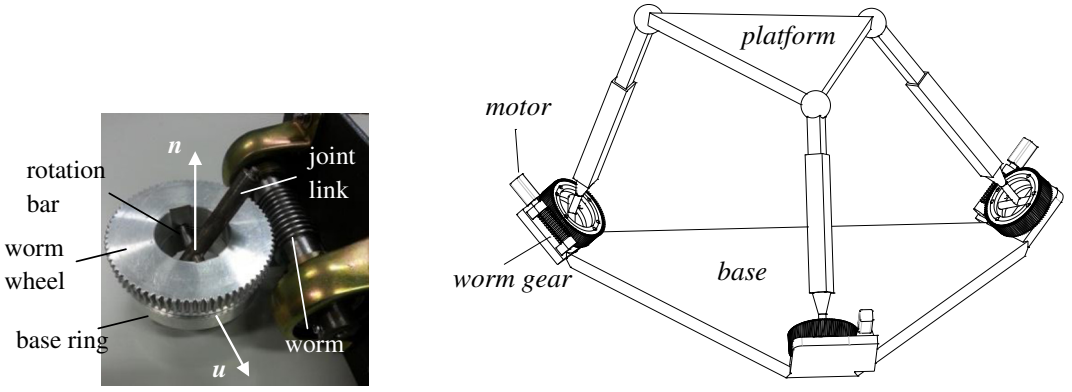

(a) rR joint using worm gear (b) 3rR*PS* using worm gear based rR joints

Fig. 12. Worm gear based independent rR joint tuning.

Please cite this article as: D. Gan, et al., Unified kinematics and optimal design of a 3rR*PS* metamorphic parallel mechanism with a reconfigurable revolute joint, Mech. Mach. Theory (2015), http://dx.doi.org/10.1016/j.mechmachtheory.2015.08.005

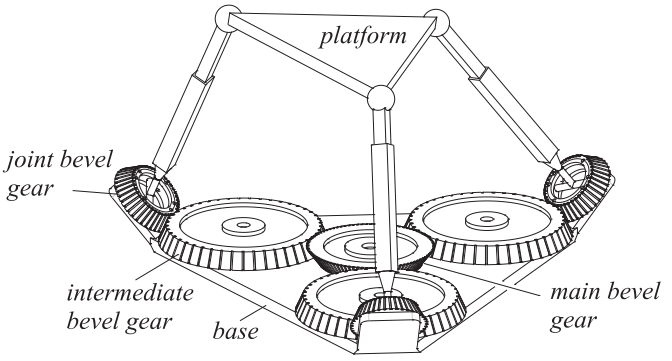

Fig. 13. Bevel gear based synchronized rR joint tuning.

perpendicular to the base ring plane. In this configuration, the base ring rotation axis passes by the spherical joint center in the limb and the rR joint tuning becomes a local limb rotation without any effect to the platform motion. At the same time, there is also no load needs to be conquered by the worm gear system which only needs a small motor for the tuning motion.

Another solution is proposed as in Fig. 13 and the rR joint reconfiguration relies on a bevel gear system. Similar to the worm gear solution, the rotation bar of the rR joint is attached to a bevel gear which can be altered by another bevel gear. In the 3rRPS MPM, a main bevel gear is used as the input with a motor input and it controls the bevel gear of the rR joint in each limb through an intermediate bevel gear as in Fig. 13. In order to save energy in reconfiguring the parallel mechanism, it needs all three limbs to be in their home positions at the same time.

It can be seen that the worm gear solution gives flexibility of controlling each rR joint independently while the bevel gear solution tunes all three limbs in a synchronized way. The former needs three small motors and the latter needs only one motor input. The bevel system will provide symmetrical rR joint axes in the 3rR*PS* MPM when the initial configuration are symmetrical. This might be preferred as generally symmetrical workspace and kinematics performance are used in applications. The worm gear system can be selected if non-symmetrical configurations are needed.

9. Conclusions

This paper introduced a reconfigurable revolute (rR) joint which qualified the new 3rR*PS* metamorphic parallel mechanism to be able to provide both 3R and 1T2R motion independently. Since the two motion types shared the same parallel mechanism structure, a unified forward kinematics solution from a 16th order polynomial in one unknown was solved analytically for both cases using the geometric constraints from the limbs. *Calay* formula representing 3D rotation was introduced to describe the mobility change resulted from the rR joints and its three Rodriguez–Hamilton parameters simplified the analysis with clear physical constraint meaning. More than that, those three parameters also showed advantages in representing singularity loci and singularity-free workspace. A multi-objective function including maximum singularity-free workspace and kinematics performance was used in optimization design of the key parameters. The results showed that a trade-off between the two criteria should be made as opposite trends were shown for the same parameter change. In addition to that, performance weights of the 3R and 1T2R topologies should be also considered as the two shared the same mechanical parameters. This was represented by a unified objective function with variable weights. Two examples were given to demonstrate the optimal design results with different performance priorities. The introduced new parallel mechanism covers the two very useful motion types 3R and 1T2R which have potential applications as machining tools, rehabilitation platforms and robotic surgery instruments. Future work will focus on the optimal design with more performance indices and a prototype implementation.

Acknowledgment

The work is partially supported by the National Natural Science Foundation of China (Project No. 51375058 and No. 51205016), the New Century Excellent Talents in University (Project No. NCET-12-0796), and the Specialized Research Fund for the Doctoral Program of Higher Education (Project No. 20120005110008).

Appendix A

Since the 1T2R topology has one translation and two rotation motions, the actuation Jacobian involves both linear and angular velocity mappings. Thus, its singular values are not in the same unit and its condition number cannot be used directly for kinematics performance evaluation. Following this, the approach of mapping the platform velocity to linear velocities in some directions at selected points on the platform representing the platform mobility [51] is used. This mapping provides a uniform unit between the linear platform point velocities and linear actuation limb inputs. To present the motion of the platform, linear velocities along $\boldsymbol{n} = (0,0,1)^{\mathrm{T}}$ at

the three spherical joint centers A_1, A_2 and A_3 are selected. Then these linear velocities can be expressed by the platform velocity in the platform coordinate frame as:

$$\boldsymbol{v}_p = [\, v_1 \quad v_2 \quad v_3 \,]^T = \mathbf{J}_p \, \mathbf{M}^{\mathrm{T}} \boldsymbol{S}_G \tag{A1}$$

where v_i is the linear velocity along $\boldsymbol{n}$ at the selected point, $\boldsymbol{J}_p = [\boldsymbol{S}_{n1} \quad \boldsymbol{S}_{n2} \quad \boldsymbol{S}_{n3}\,]^{\mathrm{T}}$, $\mathbf{M} = \begin{bmatrix} \mathbf{R} & 0 \\ 0 & \mathbf{R} \end{bmatrix}$, $\boldsymbol{S}_{ni} = [\boldsymbol{n} \quad \boldsymbol{a}'_{ii} \times \boldsymbol{n}]^T$, $(i = 1, 2, 3)$, $\boldsymbol{a}'_i$ is the vector of point A_i at which linear velocities are selected.

From Eq. (20), there is

$$\mathbf{J}\,\boldsymbol{S}_G = \begin{bmatrix} \mathbf{J}_a \\ \mathbf{J}_c \end{bmatrix} \boldsymbol{S}_G = \begin{bmatrix} 0 \\ 0 \\ 0 \\ \dot{l}_1 \\ \dot{l}_2 \\ \dot{l}_3 \end{bmatrix} = \begin{bmatrix} 0 \\ \dot{\boldsymbol{l}}_a \end{bmatrix}. \tag{A2}$$

Then

$$\boldsymbol{S}_G = \left(\mathbf{J}^{\mathrm{T}}\mathbf{J}\right)^{-1} \mathbf{J}_a^{\mathrm{T}} \dot{\boldsymbol{l}}_a. \tag{A3}$$

Combining Eqs. (A1) and (A3), the selected linear velocities can be obtained directly from the linear actuation input velocities:

$$\boldsymbol{v}_p = \mathbf{J}_p \mathbf{M}^{\mathrm{T}} \left(\mathbf{J}^{\mathrm{T}}\mathbf{J}\right)^{-1} \mathbf{J}_a^{T} \dot{\boldsymbol{l}}_a = \mathbf{J}_D^{-1} \dot{\boldsymbol{l}}_a \tag{A4}$$

where $\mathbf{J}_D = (\mathbf{J}_p \mathbf{M}^{\mathrm{T}} (\mathbf{J}^{\mathrm{T}}\mathbf{J})^{-1} \mathbf{J}_a^{\mathrm{T}})^{-1}$ is the 3×3 dimensional homogeneous Jacobian matrix with unified unit.

For the 3R topology, the unit of the Jacobian matrix is unified so it can be directly obtained from Eq. (20) as:

$$\mathbf{J}_{a3R} = \begin{bmatrix} \boldsymbol{b}_1 \times \boldsymbol{s}_1 & \boldsymbol{s}_1 \\ \boldsymbol{b}_2 \times \boldsymbol{s}_2 & \boldsymbol{s}_2 \\ \boldsymbol{b}_3 \times \boldsymbol{s}_3 & \boldsymbol{s}_3 \end{bmatrix}. \tag{A5}$$

The condition number of $\mathbf{J}_{\mathrm{D}}$ and $\mathbf{J}_{a3R}$ are used in the optimal design.

References

[1] V.E. Gough, Automobile stability, control, and tyre performance, Proc. Automob. Div., Inst. Mech. E. 171 (1956) 392–394.
[2] T. Huang, M. Li, X.M. Zhao, J.P. Mei, D.G. Chetwynd, S.J. Hu, Conceptual design and dimensional synthesis of 3-DOF module of the TriVariant—a novel 5-DOF reconfigurable hybrid robot, IEEE Trans. Robot. 21 (3) (2005) 449–456.
[3] T. Huang, J.S. Wang, D.J. Whitehouse, Closed form solution to the workspace of hexapod-based virtual axis machine tools, ASME J. Mech. Des. 121 (1) (1999) 26–31.
[4] J.S. Dai, D.R. Kerr, Six-component contact force measurement device based on the Stewart platform, Proc. Inst. Mech. Eng., Part C, J. Mech. Eng. Sci. 214 (5) (2000) 687–697.
[5] J.A. Saglia, J.S. Dai, D.G. Caldwell, Geometry and kinematic analysis of a redundantly actuated parallel mechanism that eliminates singularities and improves dexterity, ASME, J. Mech. Des. 130 (2008) 1–5, 12450.
[6] G. Brandt, A. Zimolong, L. Carrat, P. Merloz, H.W. Staudte, S. Lavallee, K. Radermacher, G. Rau, CRIGOS: a compact robot for image-guided orthopedic surgery, IEEE Trans. Inf. Technol. Biomed. 3 (4) (1999) 252–260.
[7] J.P. Merlet, Parallel Robots, 2nd Edition, Springer, 2008.
[8] D.M. Gan, Q.Z. Liao, J.S. Dai, S.M. Wei, Design and kinematics analysis of a new 3CCC parallel mechanism, Robotica 28 (7) (2010) 1065–1072.
[9] I.M. Chen, S.H. Li, A. Cathala, Mechatronic design and locomotion of Amoebot—a metamorphic underwater vehicle, J. Robot. Syst. 20 (6) (2003) 307–314.
[10] D.M. Gan, J.S. Dai, Q.Z. Liao, Mobility analysis of two types of metamorphic parallel mechanisms, ASME J. Mech., Robot. 1 (2009) 1–9, 041007.
[11] D.M. Gan, Q.Z. Liao, J.S. Dai, S.M. Wei, L.D. Seneviratne, Forward displacement analysis of a new 1CCC-5SPS parallel mechanism using Grobner theory, Proc. IMechE, Part C: J. Mechanical Engineering Science 223 (C5) (2009) 1233–1241.
[12] C. Gosselin, E. St-Pierre, M. Gagné, On the development of the Agile Eye: mechanical design, control issues and experimentation, IEEE Robot. Autom. Mag. 3 (4) (1996) 29–37.
[13] P. Vischer, R. Clavel, Argos: a novel 3-dof parallel wrist mechanism, Int. J. Robot. Res. 19 (1) (2000) 5–11.
[14] J. Hofschulte, M. Seebode, W. Gerth, Parallel manipulator hip joint for a bipedal robot, Climbing and Walking Robots, Springer, New York, 2004 601–609.
[15] T. Li, S. Payandeh, Design of spherical parallel mechanisms for application to laparoscopic surgery, Robotica 20 (2) (2002) 133–138.
[16] J. Dai, T. Zhao, C. Nester, Sprained ankle physiotherapy based mechanism synthesis and stiffness analysis of rehabilitation robotic devices, Spec. Issue Rehabil. Robot., Auton. Robot. 16 (2) (2004) 207–218.
[17] N.A. Pouliot, M.A. Nahon, C.M. Gosselin, Motion simulation capabilities of three-degrees-of-freedom flight simulators, J. Aircr.s 35 (1) (1988) 9–17.
[18] J.P. Merlet, Micro parallel robot MIPS for medical applications, Proceedings of the 8th International Conference on Emerging Technologies and Factory Automation, Antibes-Juan les Pins, France, 2001.
[19] D. Liu, R. Che, Z. Li, X. Luo, Research on the theory and the virtual prototype of 3-DOF parallel-link coordinating-measuring machine, IEEE Trans. Instrum. Meas. 52 (1) (2003) 119–125.
[20] X.J. Liu, I.A. Bonev, Orientation capability, error analysis and dimensional optimization of two articulated tool heads with parallel kinematics, ASME J. Manuf. Sci. Eng. 130 (1) (2008) 011015.
[21] J.S. Dai, J.J. Rees, Mobility in metamorphic mechanisms of foldable/erectable kinds, ASME J. Mech. Des. 121 (3) (1999) 375–382.

Please cite this article as: D. Gan, et al., Unified kinematics and optimal design of a 3r*RPS* metamorphic parallel mechanism with a reconfigurable revolute joint, Mech. Mach. Theory (2015), http://dx.doi.org/10.1016/j.mechmachtheory.2015.08.005

[22] J.S. Dai, D. Wang, Geometric analysis and synthesis of the metamorphic robotic hand, ASME J. Mech. Des. 129 (11) (2007) 1191–1197.
[23] M. Leonesio, G. Bianchi, P. Manara, A general approach for self-locking analysis in closed kinematic chains, Proceedings of the 12th World Congress in Mechanism and Machine Theory, Besancon, France 2007, pp. 141–147 (Jun).
[24] B.G. Winder, S.P. Magleby, L.L. Howell, Kinematic representations of pop-up paper mechanisms, ASME J. Mech. Rob. 1 (2) (2009) 021009.
[25] D. Zlatanov, I.A. Bonev, C.M. Gosselin, Constraint singularities of parallel mechanisms, Proc. IEEE Int. Conf. Robot. Autom., Washington, D.C. 2002, pp. 496–502.
[26] K. Wohlhart, Kinematotropic linkages, In: Lenarcic J. Parenti-Castelli V., Advances in Robot Kinematics, Kluwer, Dordrecht, 1996 pp. 359–368.
[27] P. Fanghella, C. Galletti, E. Giannotti, Parallel robots that change their group of motion, Lenarčič J. Parenti-Castelli V., Advances in Robot Kinematics: Mechanisms and Motion, Springer, Dordrecht 2006, pp. 49–56.
[28] S. Refaat, J.M. Hervé, S. Nahavandi, H. Trinh, Two-mode over-constrained three-Dofs rotational-translational linear-motor-based parallel-kinematics mechanism for machine tool applications, Robotica 25 (4) (2007) 461–466.
[29] X.W. Kong, C.M. Gosselin, P.L. Richard, Type synthesis of parallel mechanisms with multiple operation modes, ASME J. Mech. Des. 129 (6) (2007) 595–601.
[30] X.W. Kong, Type Synthesis of 3-DOF parallel manipulators with both a planar operation mode and a spatial translational operation mode1, J. Mech. Robot. 5 (4) (2013), 041015.
[31] G. Gogu, Maximally regular T2R1-type parallel manipulators with bifurcated spatial motion, ASME J. Mech., Robot. 3 (1) (2011) 1–8, 011010.
[32] I.A. Bonev, S. Briot, P. Wenger, D. Chablat, Changing assembly modes without passing parallel singularities in non-cuspidal 3-RPR planar parallel robots, Second International Workshop on Fundamental Issues and Future Research Directions for Parallel Mechanisms and Manipulators, Montpellier, France, September 21–22, 2008.
[33] G. Pagis, N. Bouton, S. Briot, P. Martinet, Enlarging parallel robot workspace through type-2 singularity crossing, Control. Eng. Pract. 39 (2015) 1–11.
[34] P. Wenger, Cuspidal and noncuspidal robot manipulators, Spec. issue Robot. Geomet. Robot. Sensing 25 (6) (2007) 677–690.
[35] V. Arakelian, S. Briot, V. Glazunov, Increase of singularity-free zones in the workspace of parallel manipulators using mechanisms of variable structure, Mech. Mach. Theory 43 (9) (2008) 1129–1140.
[36] S. Caro, D. Chablat, Y. Hu, Algorithm for the actuation mode selection of the parallel manipulator NAVARO, ASME 2014 International Design Engineering Technical Conferences and Computers and Information in Engineering Conference, Volume 5B: 38th Mechanisms and Robotics Conference, Buffalo, New York, USA, August 17–202014.
[37] C.H. Kuo, H.S. Yan, On the mobility and configuration singularity of mechanisms with variable topologies, ASME J. Mech. Des. 129 (2007) 617–624.
[38] D.M. Gan, J.S. Dai, Q.Z. Liao, Constraint analysis on mobility change of a novel metamorphic parallel mechanism, Mech. Mach. Theory 45 (12) (2010) 1864–1876.
[39] D.M. Gan, J.S. Dai, D.G. Caldwell, Constraint-based limb synthesis and mobility-change aimed mechanism construction, ASME, J. Mech. Des. 133 (5) (2011) 1–9, 051001.
[40] K.T. Zhang, J.S. Dai, Y.F. Fang, Topology and constraint analysis of phase change in the metamorphic chain and its evolved mechanism, ASME, J. Mech. Des. 132 (12) (2010) 1–11, 121001.
[41] K.T. Zhang, J.S. Dai, Y.F. Fang, Geometric constraint and mobility variation of two 3SvPS v metamorphic parallel mechanisms, ASME J. Mech. Des. 135 (1) (2012), 11001.
[42] D.M. Gan, J.S. Dai, Jorge Dias, L.D. Seneviratne, Unified kinematics and singularity analysis of a metamorphic parallel mechanism with bifurcated motion, ASME J. Mech., Robot. 5 (3) (2013) 1–11, 041104.
[43] D.M. Gan, J.S. Dai, Jorge Dias, L.D. Seneviratne, Reconfigurability and unified kinematics modeling of a 3rTPS metamorphic parallel mechanism with perpendicular constraint screws, Robot. Comput. Integrated Manuf. 29 (4) (2013) 121–128.
[44] L. Carbonari, M. Callegari, G. Palmieri, M.-C. Palpacelli, A new class of reconfigurable parallel kinematic machines, Mech. Mach. Theory 79 (2014) 173–183.
[45] J.S. Dai, J.J. Rees, Interrelationship between screw systems and corresponding reciprocal systems and applications, Mech. Mach. Theory 36 (2001) 633–651.
[46] O. Bottema, B. Roth, Theoretical Kinematics, North-Holland Publishing Company, North-Holland, New York, 1979.
[47] J.S. Dai, Finite displacement screw operators with embedded Chasles' motion, ASME J. Mech., Robot. 4 (4) (2012) 1–9, 041002.
[48] X.W. Kong, C.M. Gosselin, Uncertainty singularity analysis of parallel manipulators based on the instability analysis of structures, Int. J. Robot. Res. 20 (1) (2001) 847–856.
[49] Z. Huang, Y.F. Fang, Kinematic characteristics analysis of 3-DOF in-parallel actuated pyramid mechanisms, Mech. Mach. Theory 31 (8) (1996) 1009–1018.
[50] T. Sun, Y. Song, Y. Li, J. Zhang, Workspace decomposition based dimensional synthesis of a novel hybrid reconfigurable robot, ASME J. Mech., Robot. 2 (2010) 1–8, 031009.
[51] H. Liu, T. Huang, D.G. Chetwynd, A method to formulate a dimensionally homogeneous Jacobian of parallel manipulators, IEEE Trans. Robot. 27 (1) (2011) 150–156.

Please cite this article as: D. Gan, et al., Unified kinematics and optimal design of a 3r*RPS* metamorphic parallel mechanism with a reconfigurable revolute joint, Mech. Mach. Theory (2015), http://dx.doi.org/10.1016/j.mechmachtheory.2015.08.005